Annales Geophysicae

HF-induced airglow at magnetic zenith: theoretical considerations

E. V. Mishin[1], W. J. Burke[2], and T. Pedersen[2]

[1]Boston College, Institute for Scientific Research, Chestnut Hill, Massachusetts, USA
[2]Air Force Research Laboratory, Space Vehicles Directorate, Hanscom Air Force Base, MA 01731, USA

Abstract. Observations of airglow at 630 nm (red line) and 557.7 nm (green line) during HF modification experiments at the High Frequency Active Auroral Research Program (HAARP) heating facility are analyzed. We propose a theoretical framework for understanding the generation of Langmuir and ion acoustic waves during magnetic zenith injections. We show that observations of HF-induced airglow in an underdense ionosphere as well as a decrease in the height of the emitting volume are consistent with this scenario.

Key words. Space plasma physics (active perturbation experiments; nonlinear phenomena; wave-wave interactions)

1 Introduction

It is well known that injections of high-power, high-frequency (HF) radio waves strongly perturb ionospheric plasmas. The excitation of airglow at 630.0 and 557.7 nm is a distinctive, visual feature of such HF-induced perturbations (e.g. Sipler et al., 1974; Bernhardt et al., 1989; Pedersen and Carlson, 2001; Gustavsson et al., 2001, 2002; Kosch et al., 2000, 2002a,b; Pedersen et al., 2003). The red (r) and green (g) lines are emitted by atomic oxygen in the $O(^1D)$ and $O(^1S)$ states with the excitation energies $\varepsilon_r=1.96$ eV and $\varepsilon_g=4.17$ eV, respectively.

Significantly, green-to-red ratios $\varsigma_{gr}>0.3$ are often observed. Gustavsson et al. (2002) emphasized that $\varsigma_{gr}>0.1$ requires unrealizable electron temperatures $T_e>2$ eV, pointing out the importance of electron acceleration in the high-energy tail. The latter stems from resonant interactions with plasma turbulence generated by heater waves. Stochastic interactions heat the bulk of electrons (e.g. Gurevich et al., 1985; Dimant et al., 1992; Mantas and Carlson, 1996; Gurevich and Milikh, 1997; Istomin and Leyser, 2003). Both effects are well documented (e.g. Carlson et al., 1982; Gustavsson et al., 2001; Rietveld et al., 2003).

Observations from the heating facilities at Tromsø ($\simeq 69.7°$ N, $\simeq 18.9°$ E) and Gakona, Alaska ($\simeq 62.4°$ N,

145.15° W) show that the HF-induced airglow maximizes during injections toward magnetic zenith (MZ) (Kosch et al., 2002a; Pedersen et al., 2003). The same is true for the intensity of Langmuir waves (Isham et al., 1999) and electron heating (Rietveld et al., 2003; Dhillon and Robinson, 2003) observed by the EISCAT UHF ($f_0=933$ MHz) radar. Furthermore, the red line at MZ is excited at extremely low effective radiative power (ERP) $P_0\sim 2$ MW (Pedersen et al., 2003). The power of ion acoustic waves observed by the EISCAT UHF radar was found to be enhanced at, and 6° to the south of, MZ (Dhillon and Robinson, 2003).

The generation of Langmuir (l) and ion acoustic waves in HF modification experiments is usually explained in terms of the parametric decay (PDI) or oscillating two-stream (OTSI) instabilities of ordinary (o) mode heating waves (Fejer, 1979). However, o-mode waves with incident angles θ_0 outside the Spitze region, $\theta_0>\theta_c$, reflect at altitude H_{mz} a few km below the "standard" reflection altitude H_0, where the local plasma frequency $f_p(H_0)\simeq 10^4\sqrt{n_e(H_0)}$ Hz equals the injected frequency f_0. Here, $\theta_c=\arcsin(\sqrt{\frac{f_c}{f_c+f_0}}\sin\chi)$, f_c is the electron gyrofrequency at an altitude of 200 km, n_e is the electron density in cm^{-3}, and χ is the conjugate of the magnetic dip angle. Figure 1 shows a schematic of regions near o-mode reflection at geographic (GZ) and magnetic zenith at Gakona for $f_0=7.8$ MHz.

For a heater ERP $P_0=150$ MW and distance $R=250$ km, the wave amplitude is $E_0\simeq 5.5\sqrt{P_0}/R\simeq 0.27$ V/m (swelling is absent). With $\tilde{f}_0=f_0$[MHz]=6 and $T_e=0.1$ eV, the HF energy density at the reflection point is $W_0=\frac{E_0^2}{4\pi}\sim 10^{-4}n_eT_e$. It is sufficient to drive the PDI at H_0 (Fejer, 1979) but is not enough for injections toward MZ due to a mismatch of frequencies at H_{mz} and beneath.

Gurevich et al. (2002) suggested that decreased plasma densities, within striations generated by heating waves, permit the phase matching necessary for the PDI/OTSI to develop. Istomin and Leyser (2003) showed that electrons can be accelerated by upper hybrid waves trapped inside striations. Changes in the refraction index (self-focusing), caused by striations that form within tens of seconds after turn-on, explain some features of the spatial distribution of the
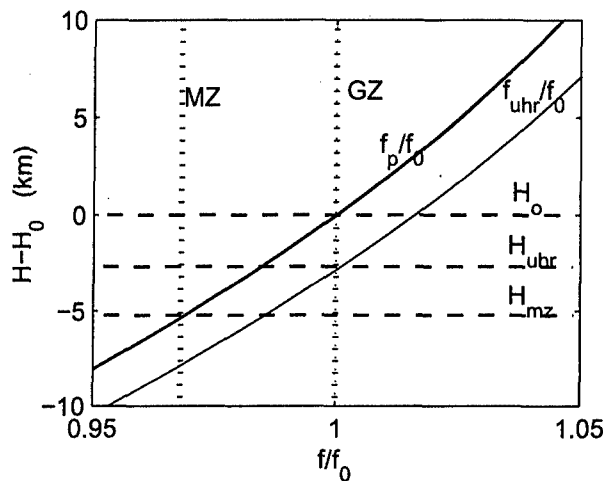
Fig. 1. Schematic of regions near ordinary-mode reflection for vertical and magnetic field-aligned heater pointings. Solid lines designate the plasma (heavy line) and upper hybrid resonance (thin) frequencies; vertical dotted lines show the cutoff frequencies at GZ and MZ, respectively; horizontal dashed lines indicate the heights of reflection at GZ, the upper hybrid resonance, and MZ.

HF-induced airglow. Kosch et al. (2002b) showed that the intensity of red-line emissions decreased when the heating frequency approached an electron gyro-harmonic, pointing out the importance of upper hybrid turbulence at MZ.

On the other hand, Langmuir waves at MZ were seen within ~10 ms (Isham et al., 1999). In 5-s resolution observations made by Dhillon and Robinson (2003), the initial increase in UHF backscatter, characterized by an overshoot, was seen coincident with the heater turn-on. Electron temperatures generally increased at heater turn-on, but the maximum increase occurred several seconds later. Mishin et al. (2004) show that during injections toward magnetic zenith the intensities of the green-line emission gained ~5 R (Rayleighs) within ~1 s. This period is dubbed the onset of HF-induced airglow. Time scales $\lesssim 1$ s appear too short for significant striations to develop (e.g. Gondarenko et al., 1999).

Striations are generated near the upper hybrid resonance height H_{uhr}, where $f_0 = f_{\mathrm{uhr}} = \sqrt{f_p^2 + f_c^2}$ (e.g. Vaskov et al., 1981; Lee and Kuo, 1983). Hence, the reflection height of an obliquely-injected heating wave must be at least at the same level. For reflection to occur above H_{uhr} during MZ injections, the inequality $f_c > f_0 \cdot \sin\chi$ must be met. For MZ injections at the HAARP heating facility ($\chi \simeq 14.6°$), $H_{\mathrm{uhr}} < H_{mz}$ if $f_0 < f_0{}^\chi \simeq 5.4$ MHz. However, the strongest airglow occurred at higher f_0 values (Pedersen et al., 2003) and at altitudes well below H_0 and H_{uhr} (Kosch et al., 2002a).

Mishin et al. (2004) suggested a scenario for exciting plasma turbulence with subsequent electron heating and acceleration in the HF-illuminated region at MZ. This scenario, depicted in Fig. 2, explores the results of Kuo et al. (1997), who showed that the OTSI can be excited by upper hybrid
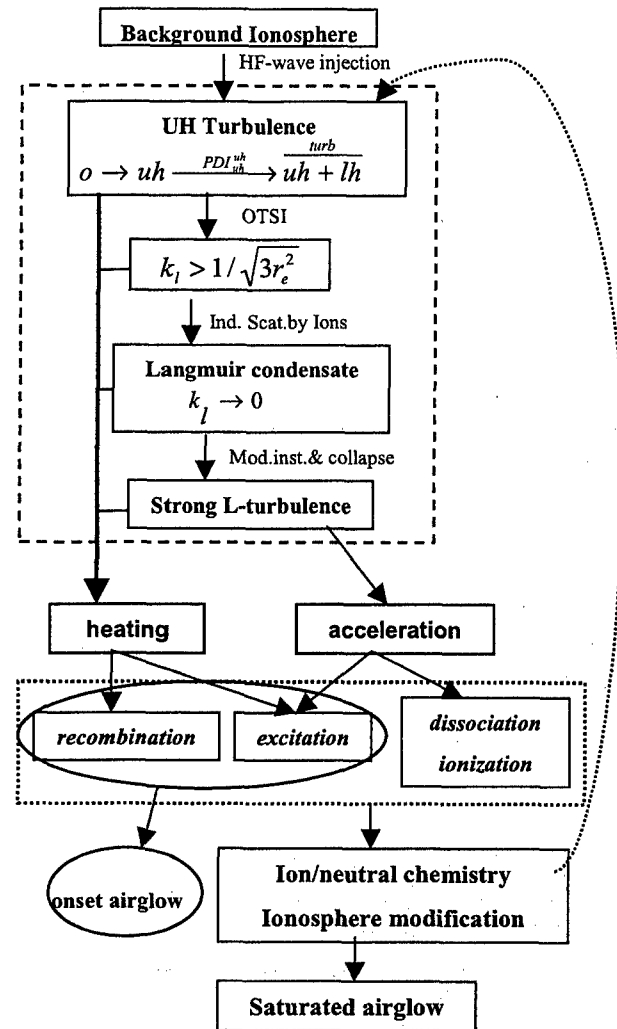

Fig. 2. Block-diagram from Mishin et al. (2004) showing energy flow in a model of HF-induced airglow at MZ. Shaded boxes indicate the steps to be worked out.

(uh) waves. In turn, uh-waves are generated through the linear conversion of the o-mode on pre-existing field-aligned irregularities (Wong et al., 1981) or by the parametric decay $o \to uh + lh$ (PDI$_o^{uh}$) (e.g. Istomin and Leyser, 1995); lh stands for lower hybrid waves.

The conversion process occurs at H_{uhr} and has no threshold. PDI$_o^{uh}$ develops if $E_0 > E_0{}^{uh} \simeq 1.6 \, \tilde{f}_0^2$ mV/m, provided the corresponding matching conditions are met for $x_{uh} = k_{uh}^2 r_e^2 < 1$. Here, r_e is the thermal electron gyroradius and k_{uh} is the uh-wave vector. Otherwise, Landau damping of short-scale lower hybrid waves raises the threshold value (Mishin et al., 1997). The rise time of the (primary) uh-wave is $\tau_{uh} \sim 1$–3 ms. When the amplitude of the primary uh-wave E_{uh} exceeds ~10 mV/m, it parametrically decays into lower frequency uh-wave (Zhou et al., 1994). The same is true for subsequently-generated uh-waves.

The OTSI excited by uh-waves produces short-scale, $k_l > 3^{-1/2}/r_e$, Langmuir waves (Kuo et al., 1997). These waves saturate via spectral transfer toward small k_l, due to induced scattering by ions (e.g. Zakharov et al., 1976). Depending on the energy density of the uh-turbulence, which depends on the ERP, the induced scattering process may deliver the Langmuir wave energy W_l to the region $k_l \to 0$ (Langmuir condensate) (Zakharov et al., 1976). The dynamics of the Langmuir condensate is defined by the modulational instability and collapse, leading to the establishment of strong (cavitating) Langmuir turbulence (e.g. Zakharov, 1972). This makes the generation of Langmuir turbulence possible within ~10 ms, consistent with the Isham et al. (1999) observations.

Collisional damping of high-frequency plasma waves is the major source of electron heating. Resonant lh- and l-wave-particle interactions accelerate electrons. Based on this scenario, Mishin et al. (2004) developed an explanatory model for the growth of emissions from MZ within the first few seconds after the HF transmitter turn on (airglow onset). The model accounts for the roles played by ambient photoelectrons and dissociative recombination of oxygen ions and shows that heating and acceleration of ambient electrons can explain the observed features of the airglow onset at MZ.

A consistent theory of the HF-induced airglow, accounting for the ion/neutral chemistry, modification of the heated spot, and self-focusing, has yet to be worked out. Pedersen et al. (2003) mentioned that the brightest emissions had a slight tendency to occur very near the critical frequency of the F-layer foF2 , but all emissions cut off sharply at about 0.5 MHz above foF2.

This paper continues our analysis of optical data acquired during the February 2002 campaign at the HAARP heating facility. We focus on intervals when foF2 dropped below the heating frequency, but HF-induced green and red lines at MZ remained. We characterize such events as the HF-induced airglow in an underdense ionosphere and show that this feature can be understood in terms of the above scenario.

2 Airglow at HAARP in the underdense ionosphere

Figure 3 shows all-sky images of the HF-induced red- and green-line emissions observed from the HAARP site during a long, ~30 min, pulse that began at 04:32:12 UT on 13 February 2002 (Pedersen et al., 2003). The data show one of the most intense green-line emissions observed at HAARP. During this (twilight) period o-mode waves were injected toward magnetic zenith at $f_0 = 7.8$ MHz and at full power of 940 KW (ERP $P_0 \simeq 165$ MW). Exposure durations were 7.5 s.

Figure 4 (top panel) shows the variation of the red- and green-line intensities in the course of the long pulse. The data points are from two red line exposures made at 0 and 24 s after each minute, with one 557.7 nm exposure at 12 s. Simultaneous observations from a digisonde located at the HAARP site showed that the reflection height of a 7.8-MHz o-mode wave at MZ gradually increased from $H_{mz} \sim 235$ to

~270 km between 04:30 and 04:50 UT. At the same time, the shadow height at the HAARP site increased from ~230 to ~300 km following the increasing solar zenith angle and so does the height of the F-peak hmF2. The magnetic conjugate point was sunlit, maintaining a flux of energetic photoelectrons (e.g. Doering et al., 1975; Peterson et al., 1977) above HAARP most of the time.

To account for natural (background) variations, a polynomial fit was made to intensities measured along the magnetic meridian in each all-sky image, with the heated area blocked out. The heater-induced airglow is determined as the difference $\Delta_\lambda = I_\lambda - b_\lambda$ between the airglow from the heated volume I_λ and the background airglow b_λ. During heater-off periods, $\Delta_\lambda^{(off)}$ was less than ~3–5 and ~7–10 R for green- and red-line emissions, respectively. This small difference determines the accuracy of heater-induced airglow measurements.

The critical frequency of the F-layer is determined from 5-min digisonde observations at the HAARP site. Apparently, foF2 dropped below the transmitter frequency in the course of this pulse. However, the airglow did not diminish. Figure 5 shows that the HF-induced airglow disappeared only at foF2 $< fo$F2$^c \simeq f_0 - 0.5$ MHz. A remark is in order. One can argue that the HAARP digisonde points vertically and the actual foF2 at H_{mz}, that is about 50 km to the south of the local vertical, might be significantly different. However, this is unlikely, for the local geophysical conditions were very quiet. This conjecture is supported by the small difference between the airglow from the heated volume during heater-off periods and the (barely changing) background airglow about 50 km apart.

In addition to Figs. 3 and 5, Fig. 6 shows the results of a survey of all the airglow-events with a 50-R or more enhancement in red line emissions observed on clear-sky nights during the February 2002 optics campaign. Apparently, for $f_0 \geq 5.8$ MHz airglow is enhanced by heating waves until foF2 $\geq fo$F2^c. No enhancements were observed at foF2 $< fo$F2^c. At $f_0 = 4.8$ and 4.5 MHz the cutoff frequency coincides with f_0 accurate to within ± 0.1 MHz, that is within the accuracy of determination of foF2. It is worth mentioning that the difference between $f_p(H_{mz}(f_0))$ and $f_0 = 7.8$, 6.8, 5.8, and 4.8 MHz is about -0.24, -0.2, -0.17, and -0.14 MHz, respectively.

3 Discussion

Mishin et al. (2004) emphasized that the scenario in Fig. 2 works at and below the reflection layer H_{mz} , provided that the matching conditions for PDI$_o^{uh}$ (e.g. Istomin and Leyser, 1995) are satisfied at local values of $x_{uh} = k_{uh}^2 r_e^2 < 1$. During injections toward MZ standing waves do not form, and the heating wave amplitude at the reflection point does not increase relative to that at lower altitudes. Thus, the reflection layer does not stand out as it does for injections within the Spitze region, where the Airy pattern is formed.
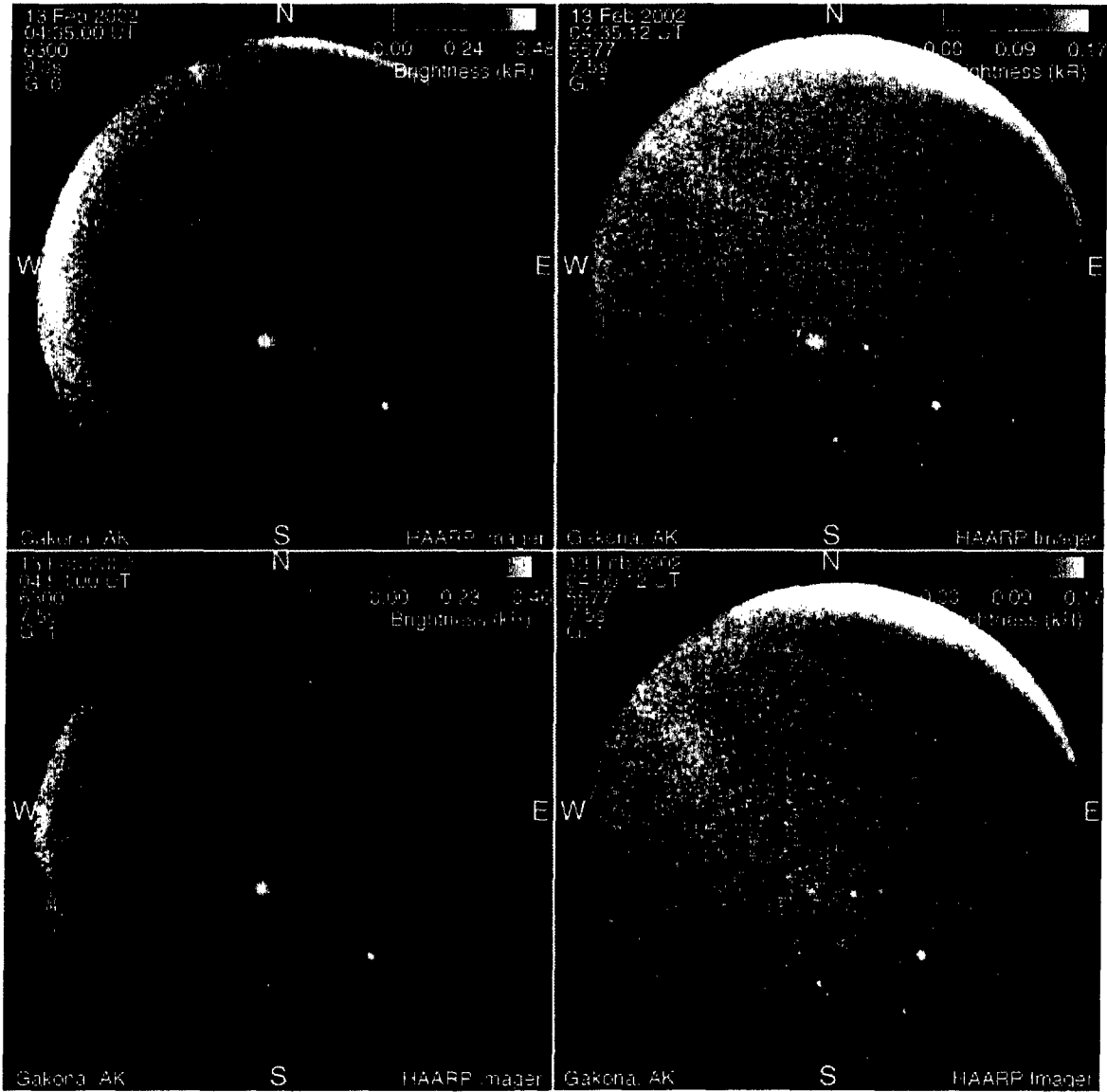
Fig. 3. Heater-induced red- and green-line emissions during the long pulse before (top) and after (bottom) f_oF2 has dropped below f_0. Bold circles mark the heated spot at MZ. Bright dots outside the circles are stars. The color bars show the brightness from 0 to 0.48 kR and from 0 to 0.17 kR for the red- and green-line emissions, respectively.

The ERP and angular width of the HF beam from the HAARP heater depend on the radiated frequency. Roughly, one can estimate $P_0 \propto f_0^2$, while the beam has full width at half maximum $\sim 27°$ and $\sim 15°$ N-S at 3.3 MHz and at 7.8 MHz, respectively. For f_0=7.8, 6.8, 5.8, 4.8, and 4.5 MHz, the free space field of the incident wave from the HAARP heater is $E_0 \simeq 0.25$, 0.2, 0.18, 0.15, and 0.14 V/m, that is $E_0 > E_0^{uh}(f_0)$.

From the dispersion relation of uh waves

$$f_{uh}(x_{uh}) \simeq f_{uhr} + \frac{3}{2} f_c \frac{(s^2-1)}{s(s^2-4)} x_{uh} + \qquad (1)$$

$$\frac{(s^2-1)^2}{2^{s+1} s!} \frac{f_c^2}{f_{uh}(x_{uh}) - sf_c} x_{uh}^{s-1}$$

one can readily obtain the value of the uh-wave vector necessary for PDI$_o^{uh}$ to occur at a given altitude H (cf. Istomin and Leyser, 1995)

$$x_{uh}^*(H, f_0) \simeq \frac{2}{3} \frac{s(s^2-4)}{s^2-1} \frac{f_0 - f_{uhr}(H)}{f_c(H)}. \qquad (2)$$

This assumes that f_0 is no closer than $\sim 0.006 f_c$ to an electron gyro-harmonic $s \cdot f_c$ and $x_{uh} < 0.5$. Here, s is defined by rounding up the f_{uhr}/f_c ratio to the nearest integer. Given $f_c(H_{mz}) \simeq 1.37$ MHz at the HAARP site (from the IGRF geomagnetic field model), the heating frequencies amount to $\simeq f_c \cdot 5.7$, 4.96, 4.23, 3.5, and 3.3, respectively. Apparently, $f_0 - sf_c > 0.006 f_c$. At H_{mz}, corresponding s-values are 6(−),
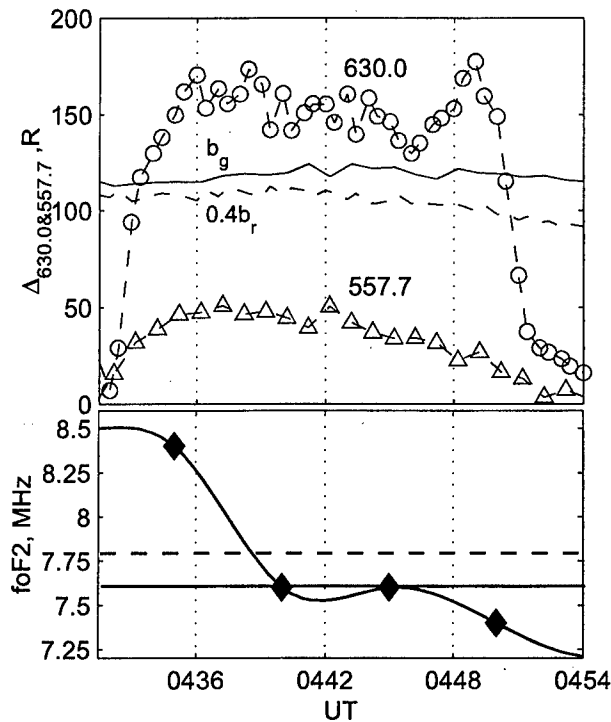
Fig. 4. Heater-induced red- and green-line emissions during the long pulse on 13 February 2002. Solid and dashed lines show intensities of the background green (b_g) and (scaled) red (b_r) emissions, respectively. (bottom) The critical frequency of the F-layer above the HAARP site (diamonds); the solid line represents a spline approximation; dashed and dotted lines show the heating frequency and the plasma frequency at H_{mz}, respectively.
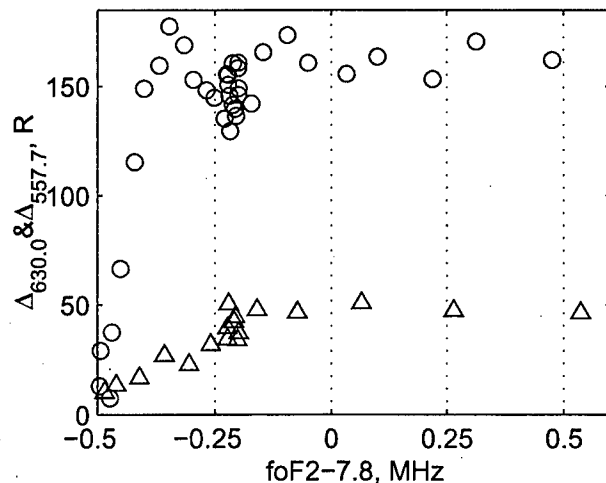

Fig. 5. Variation of the HF-induced red- (circles) and green-line (triangles) intensities with foF2 during the long pulse shown in Fig. 4.

5(−), 4(+), 4(−), and 3(+), respectively; (±) stands for the sign of $f_{uh}-sf_c$.

Let us first consider the case foF2$>f_0>f_0^\chi \simeq 5.5$ MHz, that is $H_{mz}(f_0)<H_{uhr}(f_0)$. As follows from Eq. (2), the

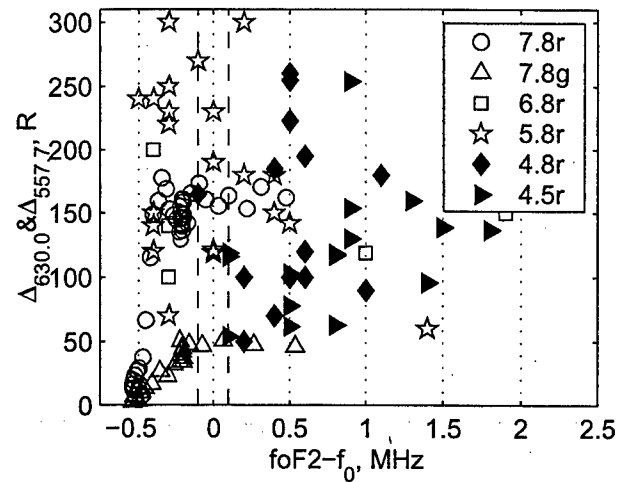**Fig. 6.** Summary plot of the variation of the HF-induced airglow at MZ with foF2$-f_0$. Here 7.8, ...4.5 stand for f_0=7.8, ...4.5 MHz; r and g indicate red- and green-line emissions; vertical dashed lines show ±0.1 MHz interval.

matching conditions for f_0=7.8, 6.8, and 5.8 MHz at the reflection height $H_{mz}(f_0)$ are satisfied at $x_{uh}^*(f_0)<0.5$. Importantly, Eq. (2) holds well below $H_{mz}(f_0)$, that is $x_{uh}^*\rightarrow1$ at $H^*(f_0)=H_{mz}(f_0)-\delta H_{mz}(f_0)$. Here, $\delta H_{mz}(f_0)$ amounts to $\simeq$3.5, 6, and 11.4 km, respectively (the gradient scale-length of a linear plasma density profile of 50 km is assumed).

The volume emission rate (VER) of the red-line emission η_r is mainly defined by the electron temperature altitude-profile (e.g. Mantas and Carlson, 1996; Mishin et al., 2004). It is very sensitive to the distribution of thermal electrons (TEDF), which may strongly deviate from a Maxwellian distribution (MD) due to inelastic collisions with molecular nitrogen N_2 (Mishin et al., 2000). For n_e given, the TEDF-MD-deviation decreases with altitude as well as collisional deactivation of the $O(^1D)$ state. Both effects provide increasing $\eta_r(T_e)$ in the course of the twilight observations (Mishin et al., 2000, 2004). Thus, following H_{mz}, the red-line intensity is expected to rise when H_{mz} approaches $hmF2$ or foF2$\rightarrow f_p(H_{mz})$.

On the other hand, the VER of the green-line emission η_g is dominated by suprathermal electrons and increases at lower altitudes (Mishin et al., 2004). Therefore, the green-line intensity is expected to decrease when foF2 approaches $f_p(H_{mz})$. These conjectures are consistent with data in Figs. 5 and 6.

As heating frequencies diminish with time, following foF2, the heated volume rises following $\delta H_{mz}(f_0)$. Thus, for the same ERP, P_0, one should expect $\Delta_{630.0}(f_0)$ to increase with decreasing $f_0>f_0^\chi$ in an underdense ionosphere. Indeed, from Fig. 6 follows that $\Delta_{630.0}(5.8)>\Delta_{630.0}(6.8)$ and $\Delta_{630.0}(7.8)$ even despite the dependence $P_0\propto f_0^2$.

After foF2 drops below $f_p(H_{mz})$, heating waves injected toward MZ are not reflected. The only consequence is that diminishing $f_{uhr}(H)$ causes $x_{uh}^*(H)$ (Eq. (2)) to increase.

1. REPORT DATE (DD-MM-YYYY)
13-06-2005

REPRINT

4. TITLE AND SUBTITLE
HF-Induced Airglow at Magnetic Zenith: Theoretical
Considerations

5a. CONTRACT NUMBER

5b. GRANT NUMBER

5c. PROGRAM ELEMENT NUMBER
61102F

6. AUTHOR(S)
E.V. Mishin*, W.J. Burke and T. Pedersen

5d. PROJECT NUMBER
2311

5e. TASK NUMBER
SD

5f. WORK UNIT NUMBER
A3

7. PERFORMING ORGANIZATION NAME(S) AND ADDRESS(ES)
Air Force Research Laboratory/VSBXP
29 Randolph Road
Hanscom AFB MA 01731-3010

8. PERFORMING ORGANIZATION REPORT NUMBER

AFRL-VS-HA-TR-2005-1058

9. SPONSORING / MONITORING AGENCY NAME(S) AND ADDRESS(ES)

10. SPONSOR/MONITOR'S ACRONYM(S)

11. SPONSOR/MONITOR'S REPORT NUMBER(S)

12. DISTRIBUTION / AVAILABILITY STATEMENT
Approved for Public Release; Distribution Unlimited.

*Institute for Scientific Research, Boston College, Chestnut Hill, MA

14. ABSTRACT

Abstract. Observations of airglow at 630 nm (red line) and
557.7 nm (green line) during HF modification experiments
at the High Frequency Active Auroral Research Program
(HAARP) heating facility are analyzed. We propose a theo-
retical framework for understanding the generation of Lang-
muir and ion acoustic waves during magnetic zenith injec-
tions. We show that observations of HF-induced airglow in
an underdense ionosphere as well as a decrease in the height
of the emitting volume are consistent with this scenario.

15. SUBJECT TERMS
Space plasma physics
Active perturbation experiments
Non-linear phenomena
wave-wave interactions

16. SECURITY CLASSIFICATION OF:

a. REPORT	b. ABSTRACT	c. THIS PAGE
UNCLAS	UNCLAS	UNCLAS

17. LIMITATION OF ABSTRACT
SAR

18. NUMBER OF PAGES

19a. NAME OF RESPONSIBLE PERSON
W. Burke

19b. TELEPHONE NUMBER (include area code)
781-377-3980